Nuclear Medicine and Molecular Imaging (2019) 53:115–124
https://doi.org/10.1007/s13139-019-00584-z

REVIEW

ISSN (print) 1869-3482
ISSN (online) 1869-3474

Progress of Coordination and Utilization of Zirconium-89 for Positron Emission Tomography (PET) Studies

Minh Thanh La[1] · Van Hieu Tran[1] · Hee-Kwon Kim[1]

Received: 14 December 2018 / Revised: 14 January 2019 / Accepted: 17 January 2019 / Published online: 29 January 2019

Abstract

Radiometals have been commonly used in medical applications, and utilization of such metals continues to be an attractive research area. In particular, a variety of radiometals have been developed and implemented for molecular imaging. For such applications, ^{89}Zr has been one of the most interesting radiometals currently used for tumor targeting. Several chemical ligands were developed as ^{89}Zr chelators, and new coordinating methods have also been developed more recently. In addition, immuno-positron emission tomography (PET) studies using ^{89}Zr-labeled monoclonal antibodies have been performed by several scientists. In this review, recent advances to the coordination of ^{89}Zr and the utilization of ^{89}Zr in PET studies are described.

Keywords ^{89}Zr · Positron emission tomography (PET) · Coordination · Ligand

Introduction

Zirconium-89 (^{89}Zr), with an atomic number of 40, has useful biomedical applications. This is due to its favorable decay characteristics, a half-life of 78.41 h, which make it suitable for labeling biomolecules, such as antibodies, for imaging (Fig. 1, Table 1). Nowadays, ^{89}Zr is considered an important positron-emitting radionuclide used for the development of novel radiopharmaceuticals for positron emission tomography (PET). In particular, ^{89}Zr has been widely used for immuno-PET studies due to ideal physical characteristics.

Production of ^{89}Zr

There are several reaction pathways that produce ^{89}Zr, such as the ^{89}Y(p,n)^{89}Zr reaction, ^{89}Y(d,2n)^{89}Zr reaction, ^{nat}Zr(p,pxn)^{89}Zr reaction, ^{nat}Sr(α,xn)^{89}Zr reaction, and ^{90}Zr(n,xn)^{89}Zr reactions (Table 2) [5, 6, 12–14]. The first two of these reactions are common pathways to produce ^{89}Zr due to the availability of ^{89}Y from natural sources. The Zweit group utilized natural yttrium pellets to produce ^{89}Zr using the ^{89}Y(d,2n)^{89}Zr reaction: the starting material was irradiated with a 16–7-MeV optimum energy beam of deuterons and then purified in an ion-exchange column to obtain a 66.6-MBq/μAh yield of ^{89}Zr with a minor fraction of long-lived ^{88}Zr (0.008%). Using a similar reaction, high-purity ^{89}Zr production was experimentally reported by Tang and co-workers and theoretically calculated by the Sadeghi group [3, 15]. Despite the higher yield of the ^{89}Y(d,2n)^{89}Zr reaction compared to the ^{89}Y(p,n)^{89}Zr reaction, application of the ^{89}Y(d,2n)^{89}Zr reaction in medical accelerators is still restricted. This is due to the fact that common small medical cyclotrons are not capable of producing the high-energy deuterons required for the ^{89}Y(d,2n)^{89}Zr reaction. Although several medical cyclotrons, such as the GE PETtrace 800 or IBA Cyclone 18/9, have two beam currents, the deuteron energy still is not sufficient to produce a high yield of ^{89}Zr. Hence, the ^{89}Y(p,n)^{89}Zr reaction is the more practical approach to the production of ^{89}Zr in these kinds of machines.

The first ^{89}Y(p,n)^{89}Zr reaction was carried out by Link and co-workers who employed an ^{89}Y source on Y foil which was irradiated with 13 MeV protons. After irradiation, the Y foil was dissolved in HCl solution, and ^{89}Zr(IV) was extracted via multistep extraction using 4,4,4-trifluoro-1-(2-thienyl)-1,3-

✉ Hee-Kwon Kim
hkkim717@jbnu.ac.kr

[1] Department of Nuclear Medicine, Molecular Imaging & Therapeutic Medicine Research Center, Cyclotron Research Center, Biomedical Research Institute, Chonbuk National University Medical School and Hospital, Jeonju, Jeonbuk 54907, Republic of Korea

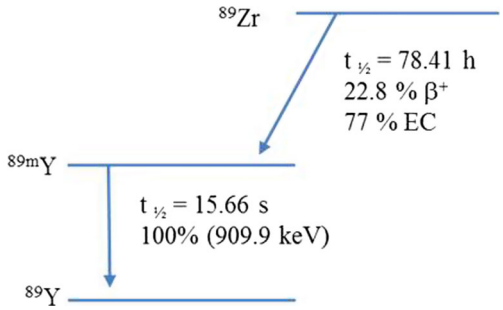

Fig. 1 Zirconium-89 decay

butanedione (TTA) and then HNO_3/HF. Purification by anion exchange with 1 M HCl/0.01 M oxalate resulted in an 80% yield of ^{89}Zr (99.99% purification). A similar protocol was reported by the Dejesus group using a thin Y foil [4, 5]. Based on the same starting material of a Y foil target, several studies modified parameters such as foil thickness, time of irradiation, energy, and beam current in the attempt to improve production yields [6–8]. However, the increase of beam energy over 13 MeV inevitably causes the undesirable production of long-lived ^{88}Zr via the ^{89}Y(p,2n)^{88}Zr reaction. Recently, the Queern group worked on the production of ^{89}Zr using sputtered yttrium on niobium coin. They found that a reduction of beam energy from 17.8 to 12.8 MeV or 12.5 MeV using a 0.75-mm-thick aluminum degrader yielded good results with no ^{88}Zr observed [10].

The use of solid targets can be limited by a lack of facilities, so liquid targets have also been utilized to produce ^{89}Zr. For instance, Pandey and co-workers irradiated yttrium (III) nitrate in nitric acid solution. Although their results showed a yield of only 4.4 MBq/μAh for 2 h of irradiation at a 40-μA beam current, which is barely adequate for a solid target, this yield was still better than what has been achieved with conventional liquid targets [11].

Coordination Chemistry and Ligands of ^{89}Zr

Desferrioxamine and Its Derivatives

In order to effectively utilize ^{89}Zr, coordination chemistry has been applied to study various chelates. The chelate first utilized for ^{89}Zr is also currently the widely used: desferrioxamine (DFO). As showed in Fig. 2, DFO, which contains three RCO-N(R′)-OH motifs, is a hydroxamate-type siderophore that chelates with ^{89}Zr to form a ^{89}Zr-DFO complex, which is used in ^{89}Zr-immuno-PET studies. Complexes with ^{89}Zr based on the iron-chelator Desferal, DFO (L23), which includes hexadentate coordination of three hydroxamate units, and its derivatives have also been used in ^{89}Zr-PET studies. However, ^{89}Zr-DFO has been known to have some disadvantages, such as poor stability. Since its hexadentate complex is not saturated by a stably octa-coordinated Zr^{4+} sphere, ^{89}Zr-DFO instability has been observed in several animal model experiments [6, 16]. Due to the importance of developing ligands for zirconium-89-based radiopharmaceuticals, especially for immuno-PET imaging, several DFO derivatives have been reported (Fig. 3), such as *N*-(*S*-acetyl) mercaptoacetyldesferal (SATA-DFO) [17] and 2,3,5,6-tetrafluorphenoxy (TFP)-*N*-succinyldesferal-Fe [18]. These modifications were prepared for bifunctional mAb coupling; however, both protocols showed several drawbacks. For example, an unstable thioether linker exists between maleimide-mAb and SATA-DFO at physiological pH and a complicated six-step reaction is used to prepare mAb-*N*-succinyldesferal-^{89}Zr, consisting of carboxylation of the amine, protection with Fe(III), activation of the ester, attachment with a mAb, deprotection of Fe(III) from complex, and labeling with ^{89}Zr radionuclide [19].

A simple two-step synthesis to prepare bifunctional ^{89}Zr-labeled mAb via *p*-isothiocyanatobenzyl-desferrioxamine (DFO-Bz-NCS) was reported by Perk and co-workers more recently. This complex was described to be stable due to the strong and steady thiourea bond between the monoclonal antibodies and the chelator. Although this process proved to be a fast and effective method to acquire ^{89}Zr-labeled mAbs, the restricted water solubility of the DFO-Bz-NCS precursor required experimental skill to prevent aggregation and precipitation of the antibody. Also, despite the stability of thiourea linker, it was reported to be easily cleaved by radiation in some buffers that contain chlorinated compounds [20, 21]. Another rapid and specific conjugation between modified-[^{89}Zr]Zr-DFO and RGP peptides by the click reaction was described by Gao and co-workers. The modification of DFO at the terminal amine with 2-cyanobenzothiazole (CBT) or 1,2-aminothiol (cys) produced [^{89}Zr]Zr-DFO-CBT or [^{89}Zr]Zr-DFO-cys, respectively. Luciferin linkage formation from the click reaction of those with their complementary functionality on RGP peptides showed a high stability with an almost intact complex upon cysteine challenge [22].

Table 1 Properties of ^{89}Zr

$t_{½}$ (h)	Methods of production	Decay mode	$E_{β+}$ (keV)	References
78.41	^{89}Y(p,n)^{89}Zr	$β^+$ (22.7%) EC (77%)	909	[1]

Table 2 Several reactions for ^{89}Zr production

No.	Nuclear reaction	Target	Product chemical form	Yield (MBq/μAh)	Time of irradiation	Energy (MeV)	Beam current (μA)	Thickness of target	Refs.
1	^{89}Y(d,2n)^{89}Zr	Pellet	Chloride	66.6 ± 5.6	12–20 min	16–7	3–5	240–340 mg cm^{-2}	[2]
2	^{89}Y(d,2n)^{89}Zr	Magnetron sputtering	Chloride	58 ± 5	1 h	13	10–15	25 μm	[3]
3	^{89}Y(p,n)^{89}Zr	Magnetron sputtering	Chloride	44 ± 4	1 h	14	10–30	25 μm	[3]
4	^{89}Y(p,n)^{89}Zr	Foil	Oxalate	38.9	40 min	13	10	286 mg cm^{-2}	[4]
5	^{89}Y(p,n)^{89}Zr	Thin foil	Oxalate	13	2 h	11.4–10	10	57 mg cm^{-2}	[5]
6	^{89}Y(p,n)^{89}Zr	Foil	Oxalate	56.2 ± 4.1	2–5 h	15	15	100 μm	[6]
7	^{89}Y(p,n)^{89}Zr	Foil	Oxalate	12.5 ± 0.5	2 h	18–10	12	150 μm	[7]
8	^{89}Y(p,n)^{89}Zr	Foil	Oxalate	48.9 ± 4.4	1 h	12.8	45	640 μm	[8]
9	^{89}Y(p,n)^{89}Zr	Sputtered layer	Oxalate	48.1	1 h	14	100	25 μm	[9]
10	^{89}Y(p,n)^{89}Zr	Sputtered coin	Oxalate	6.4–18	30 min or 2 h	12.5 or 12.8	10–40	90–250 μm	[10]
11	^{89}Y(p,n)^{89}Zr	$Y(NO_3)_3$ solution (2.75 M)	Oxalate	4.36 ± 0.48	2 h	14	40	Liquid target	[11]

Octadentate coordination using DFO-1-hydroxy-2-pyridone (DFO-HOPO) was first described by White and co-workers [23]. This study employed the DFO-HOPO ligand as a plutonium(IV) chelator for treatment of plutonium poison. Low toxicity and a stable octadentate coordination complex with Pu(IV) were observed when the 1,2-HOPO compound was introduced to the DFO molecule. Allott adopted this method and utilized DFO-HOPO to evaluate the stability of octadentate as an ^{89}Zr chelator. Results showed ^{89}Zr-DFO-HOPO to be stable compared to ^{89}Zr-DFO with no demetallation during radio-ITLC analysis, and no bone uptake of ^{89}Zr was observed within 24 h after ^{89}Zr injection. Moreover, ^{89}Zr-DFO-HOPO showed inertness to transchelation by EDTA or serum. DFO*, a modification of DFO by adding one more hydroxamic acid part, was reported as the first octadentate chelator for ^{89}Zr labeling molecules with improved stability [24, 25]. A few years later, the bifunctional chelator DFO*-pPhe-NCS was prepared as an octadentate chelator with ^{89}Zr. ^{89}Zr-DFO*-mAb demonstrated greater stability than the previous hexadentate ^{89}Zr-DFO-mAb with more than twice the intact tracer when stored at room temperature. Yet, solubility is still a challenge for the thiourea structure [26].

Other Hydroxamate-Type Chelators

To expand the utilization of hydroxamate-type coordination with ^{89}Zr, many hydroxamate-containing non-DFO structures have been developed (Fig. 4). Guérard and co-workers reported the simplest structures, acetohydroxamic acid (AHA) and its methylated derivative (Me-AHA), as ligands to coordinate with Zr(IV) and ^{89}Zr(IV). Based on X-ray crystallography and potential titration, these studies found a metal to ligand ratio of 1:4 and octadentate coordination with Zr(IV) that was supposedly better than results with DFO. Through an ^{89}Zr labeling complexation study, Me-AHA showed a better activity complex than did AHA. This can be explained by a higher electron density of the oxygen atom (N–O) of Me-AHA which forms a strong bond toward the ^{89}Zr radionuclide [27]. Recently, two bifunctional tetrahydroxamate ligands were synthesized by

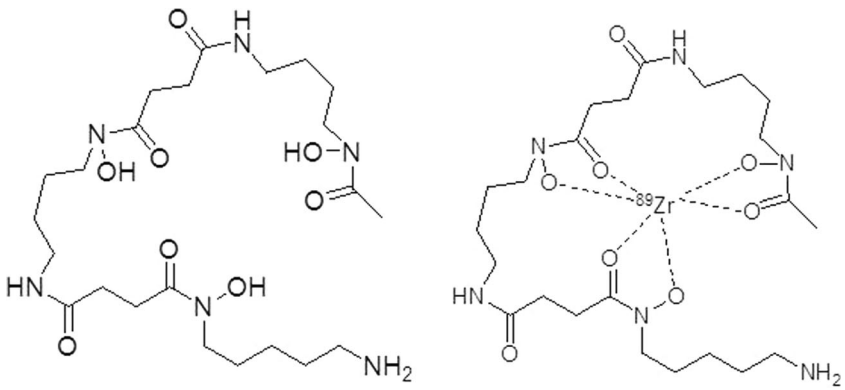

Fig. 2 Structure of DFO and its ^{89}Zr-complex

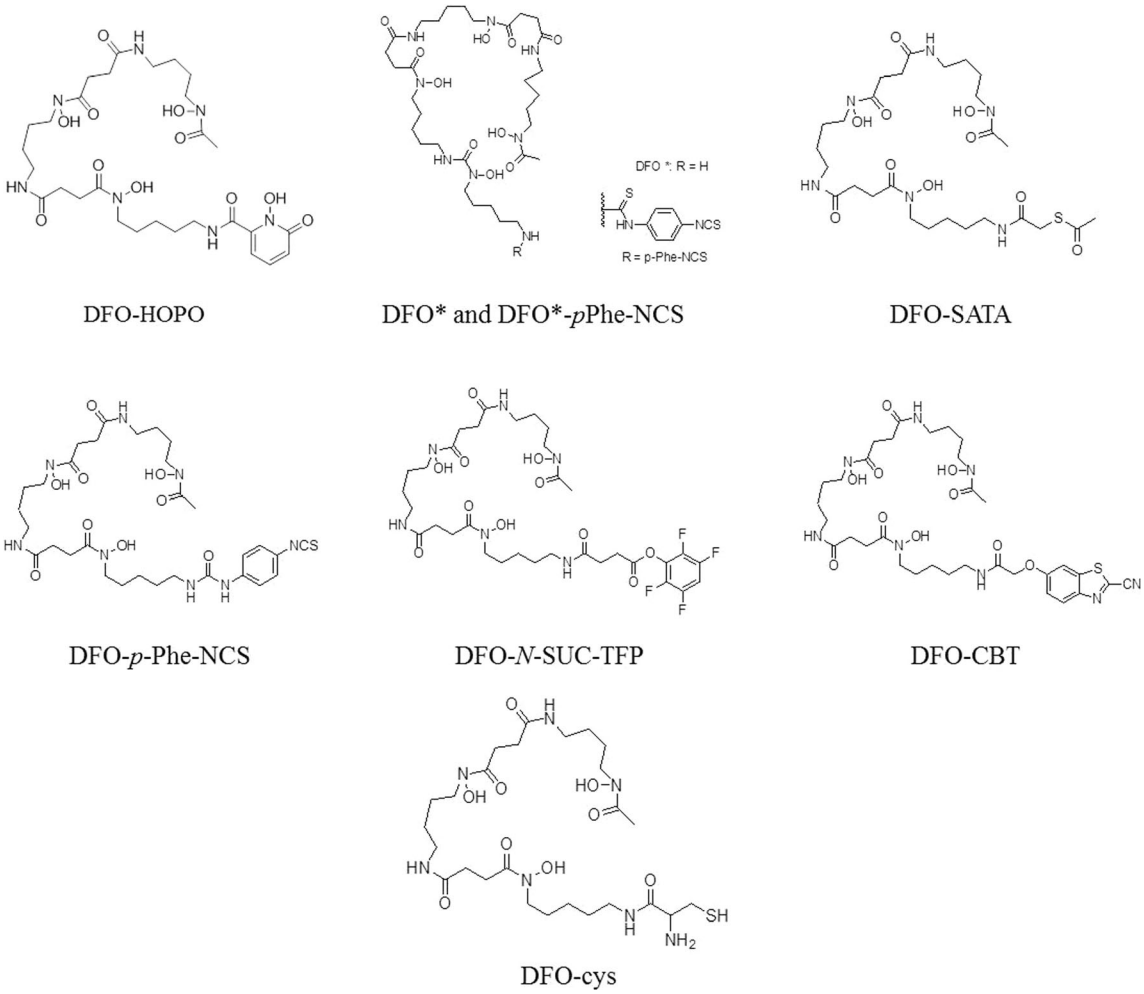

Fig. 3 DFO derivatives

Rousseau and co-workers based on an iminodipropionamide scaffold. This work was a modification of their previous study that elongated the aliphatic chain on the main ligand and reduced the distance between ligand and isothiocyanate moiety. Despite improved stability, the biodistribution and PET imaging properties of these ligands showed no significant differences compared to those this group studied previously or to DFO [28].

Macrocyclic structures including hydroxamate moieties have also been developed, such as triacetylfusarinine C (TFAC), desferrichrome (DFC), and tetrahydroxy octaazacyclohexatriacontan-octaone (CTH36). This type of ligand was reported to form steadier coordination than linear ligands. In addition, as a result of the macrocycle effect, a ligand that has a macrocyclic structure could possess an advantage due to the strong stability of the complex [29–32].

Other Types of Chelators

There is a similar structure between hydroxypyridone (HOPO) and hydroxamate; hence, HOPO was also employed as a polydentate hydroxypyridone ligand. The development of a HOPO ligand for chelating ^{89}Zr radionuclides was reported by Deri and co-workers. 3,4,3-(LI-1,2-HOPO), which has four hydroxypyridone moieties (Fig. 5), could make an octadentate ^{89}Zr complex which significantly enhances stability compared to DFO in DFT calculations. The ^{89}Zr-HOPO complex was inert to transchelation in EDTA and serum challenge tests. In serum, the ^{89}Zr complex was an almost intact radiotracer after a 7-day incubation. ^{89}Zr-HOPO also possesses satisfactory biological behavior such as rapid renal excretion and low radioactivity in bone tissue. Conjugation of ^{89}Zr-HOPO with antibodies to make bifunctional ligands is currently an active area of research [33].

Hydroxyisophthalimide (IAM) ligands, originally used for lanthanides, were also described to produce stable ^{89}Zr complexes. Bhatt group investigated two analogs of IAM, including IAM 1 and IAM 2 which differed by one pensile IAM group (Fig. 6). The result showed that the stability of ^{89}Zr-IMA 1 was greater than that of ^{89}Zr-DFO which was in turn greater than that of ^{89}Zr-IMA 2 (with 72%, 41%, and 26% tracer intact, respectively, after a 7-day incubation with

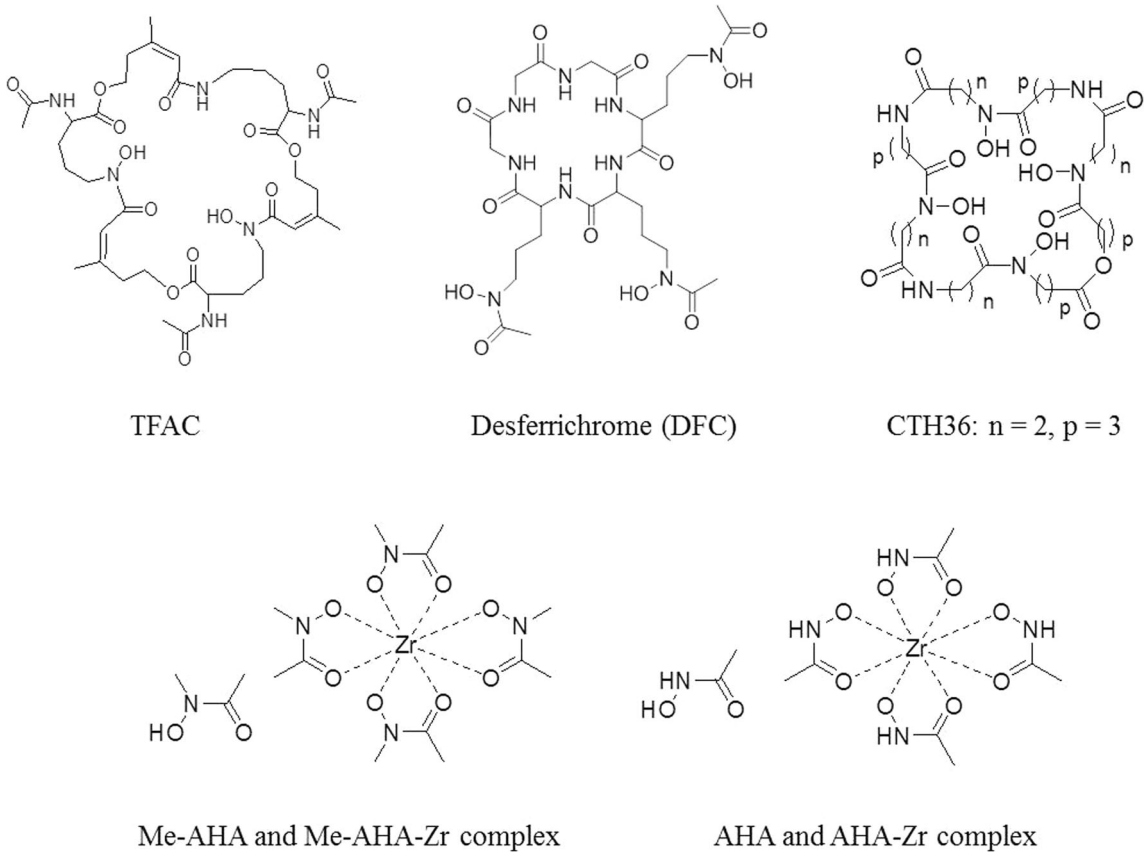

Fig. 4 Other hydroxamate-type ligands

DTPA). However, in the amino model, ^{89}Zr-IAM 1 and ^{89}Zr-IAM 2 accumulated much more in the kidneys, liver, and bone than did ^{89}Zr-DFO. ^{89}Zr-immuno-PET imaging with ^{89}Zr-IAM 1 is currently still under further investigation [34].

Ligands containing carboxylate and amino donors, such as EDTA and DTPA, have also been reported to complex with ^{89}Zr [35]. Recently, the Wadas group used various kinds of tetraazamacrocycle ligands, namely, DOTA, DOTP, and DOTAM, to react with $^{89}ZrCl_4$ to form Zr complexes (Fig. 7) [36]. The stability of resulting Zr-complexes (Zr-DOTA, Zr-DOTP, Zr-DOTAM) which were tested with an excess amount of EDTA or a high concentration of metal ions (Fe , Zn , Co , Cu , Mg , Gd , Ga) was showed as following order: Zr-DOTA >> Zr-DOTP> Zr-DOTAM> Zr-DFO. In additions, they found that Zr-DOTA was stable, showing no change even after 7 days.

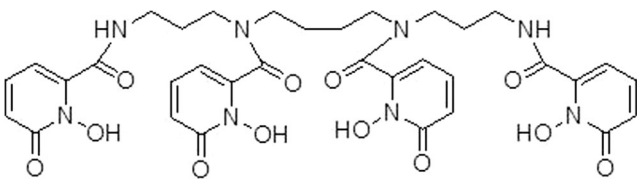

Fig. 5 Structure of 3,4,3-(LI-1,2-HOPO)

In in vivo biodistribution experiments, ^{89}Zr-DOTAM showed a large amount of radioactivity in the liver and spleen, while ^{89}Zr-DOTA showed relatively low radioactivity in the liver, kidneys, and bone. Results from ^{89}Zr-DOTP were generally similar to those from ^{89}Zr-DOTA, except that high amounts of radioactive material were found in the bone with ^{89}Zr-DOTP. Based on these results, dynamic PET imaging studies were conducted using ^{89}Zr-DOTA and ^{89}Zr-DFO. In contrast, ^{89}Zr-DFO accumulates significantly in the kidneys after 4 and until 24 h. However, ^{89}Zr-DOTA accumulates less in the kidneys and bones than does ^{89}Zr-DFO. A small amount of ^{89}Zr-DOTA was observed in the bladder at 4 h, and after 24 h, the radioactivity in the bladder was found to be negligible. Thus, it was found that ^{89}Zr-DOTA was easily cleared from the living body over a short period of time. Therefore, we confirmed that ^{89}Zr-DOTA could be effectively applied to precision medicine without the disadvantages that come with ^{89}Zr-DFO, which is currently used.

Immuno-PET Studies Using ^{89}Zr

In order to apply ^{89}Zr to precision medicine, immuno-PET studies using ^{89}Zr-labeled monoclonal antibodies (mAbs)

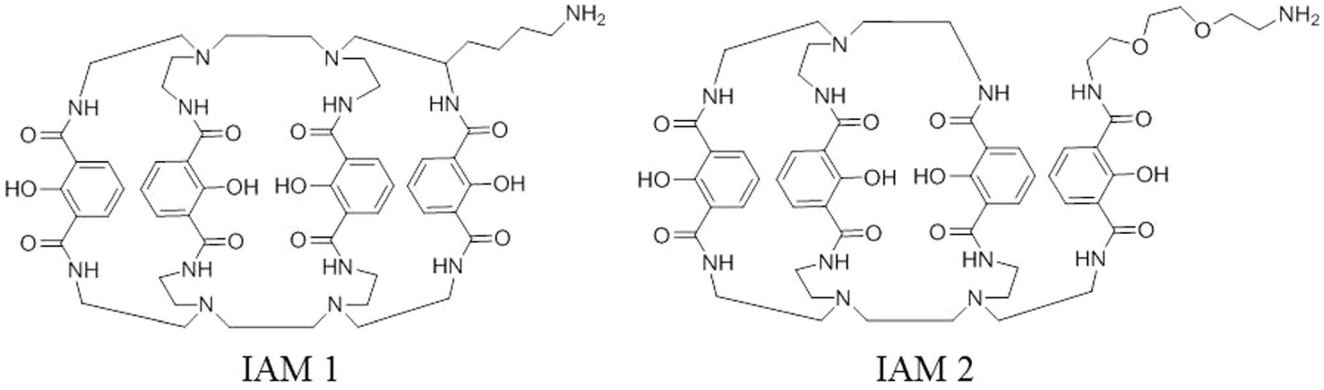

Fig. 6 Structure of hydroxyisophthalimide (IAM) ligands

have been carried out by various researchers (Table 3). For instance, measurements of metastasis in persons with breast cancer have been carried out using trastuzumab [49]. Trastuzumab is a target for human epidermal growth factor receptor 2 (HER2), which has been used to diagnose HER2-positive breast cancer, and thus, treatment with trastuzumab has shown positive results in patients with HER2-positive breast cancer and gastric cancer [50, 51]. In one case, HER2-negative early breast cancer patients were found to have HER2-positive cancer metastases with PET/CT scans using ^{89}Zr-trastuzumab (Fig. 8) [49]. In addition, ^{89}Zr-trastuzumab PET was used to evaluate the alteration of HER2 expression in patients with HER2-positive breast cancer after they were treated with the anti-angiogenic agent NVP-AUY922, the novel heat shock protein 90 (HSP90) inhibitor. This study suggested that ^{89}Zr-immuno-PET can be useful for determining the alteration of antigen expression and for monitoring the response to treatment with anti-cancer agents [52].

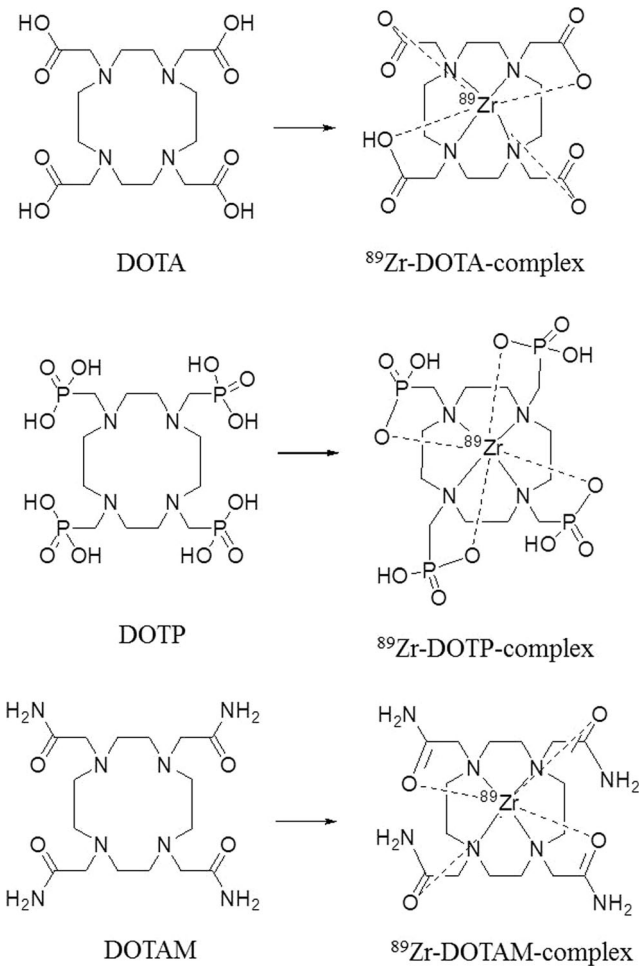

Fig. 7 Structure of tetraazamacrocylic ligands and their ^{89}Zr complexes

Studies targeting vascular endothelial growth factor A (VEGF-A) have also been conducted using ^{89}Zr-labeled mAbs [39, 40, 52–54]. VEGF-A is overexpressed in malignant breast tumors and ductal carcinoma in situ and is known to be associated with various diseases. Bevacizumab has been reported as a monoclonal antibody that targets VEGF-A, and it has been successfully utilized in several studies. In particular, ^{89}Zr-bevacizumab PET has been used for various ailments such as breast cancer, pelvic cancer, renal cell carcinoma, and neuroendocrine tumors to effectively identify the biological properties of the tumor and confirm the effectiveness of treatment (Fig. 9).

EGFR is also another interesting target antigen. Cetuximab is a widely known agent to target EGFR. Attachment of cetuximab to EGFR prohibits binding of growth factor to the receptor, and the receptor tyrosine kinase activity is prevented. Thus, biological events such as cell growth, proliferation and differentiation, and cellular invasiveness and apoptosis can be slowed or stopped. ^{89}Zr-cetuximab has been used to evaluate patients with advanced colorectal cancer; tumor uptake was investigated via checking the biodistribution of this labeled antibody [55].

Visualization of metastatic prostate cancer is critical to monitoring the treatment of metastatic prostate cancer. HuJ591 was developed for selectively targeting the extracellular domain of prostate-specific membrane antigen (PSMA), which most prostate cancers express. An immuno-PET

Table 3 Application of ^{89}Zr-mAb in clinical oncology studies

Year	mAb	Target	Tumor type	Refs.
2006	Chimeric mAb U36	CD44v6	Head and neck cancer	[37]
2012	Ibritumomab-tiuxetan	CD20	B cell lymphoma	[38]
2013	Bevacizumab	VEGF-A	Breast cancer	[39]
2014	Bevacizumab	VEGF-A	Neuroendocrine tumors	[40]
2015	Fresolimumab	TGF-β	Glioma	[41]
2016	MMOT0530A	MSLN	Pancreatic, ovarian cancer	[42]
2017	Cetuximab	EGFR	Head and neck, lung cancer	[43]
2017	Rituximab	CD20	B cell lymphoma	[44]
2017	Lumretuzumab	HER3	Multiple cancer types	[45]
2017	Bevacizumab	VEGF-A	Metastatic renal cell carcinoma	[46]
2018	Trastuzumab	HER2	Breast cancer	[47]
2018	Atezolizumab	PD-L1	Bladder cancer, non-small cell lung cancer, triple-negative breast cancer	[48]

imaging study in patients with metastatic prostate cancer using ^{89}Zr-huJ591 was performed [56]. In this case, 5 mCi of ^{89}Zr-huJ591 was injected into 10 patients, and its distribution, elimination, and lesion accumulation were examined. In the PET image, ^{89}Zr-huJ591 was found to accumulate in lesions in the bone and soft tissues more effectively than ^{99m}Tc-MDP or FDG. In particular, when analyzing images using ^{89}Zr-huJ591, 11 out of 12 lesions were positive, which proved to be superior to corresponding PET scans using FDG that yielded only 9 positive results.

Another study used ^{89}Zr-labeled cmAb U36 to detect head and neck squamous cell carcinoma (HNSCC) tumors in 20 patients. This study suggested that most of primary tumors were identified by ^{89}Zr-immuno-PET, and performance results of ^{89}Zr-immuno-PET for the detection of lymph node metastasis were no different from those of computed tomography (CT) or magnetic resonance imaging (MRI) [37].

There are no important drug targets for cancers such as pancreatic and ovarian carcinoma. However, it was reported that membrane-bound surface glycoprotein mesothelin (MSLN) is overexpressed in pancreatic and ovarian cancer. Thus, the anti-MSLN antibody MMOT0530A was discovered as a potential imaging biomarker [42, 57]. PET studies using ^{89}Zr-MMOT0530A indicated that its tumor uptake in patients with either pancreatic cancer or ovarian cancer could be clearly visualized. IHC studies suggested that MSLN expression levels, determined with IHC scores, were strongly associated with the intensity of tumor uptake of ^{89}Zr-MMOT0530A.

Conclusion

These results suggest that further study of ^{89}Zr will solve current shortcomings and contribute to molecular imaging

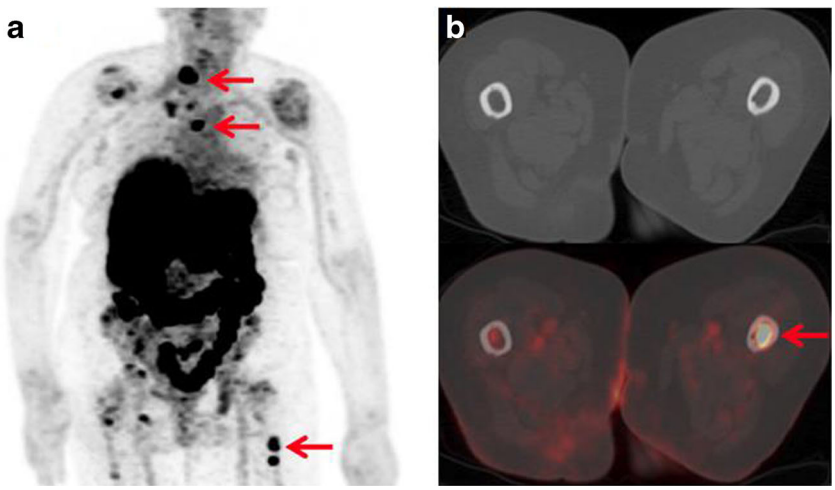

Fig. 8 Eighty-three-year-old woman with primary ER-positive/HER2-negative invasive ductal breast carcinoma. **a** ^{89}Zr-trastuzumab maximum intensity projection demonstrates several foci of ^{89}Zr-trastuzumab avidity that localize to osseous structures. **b** Axial CT and ^{89}Zr-trastuzumab PET/CT demonstrate ^{89}Zr-trastuzumab avidity in proximal left femur. Reprinted with permission from ref. [49]. Copyright 2016 Society of Nuclear Medicine

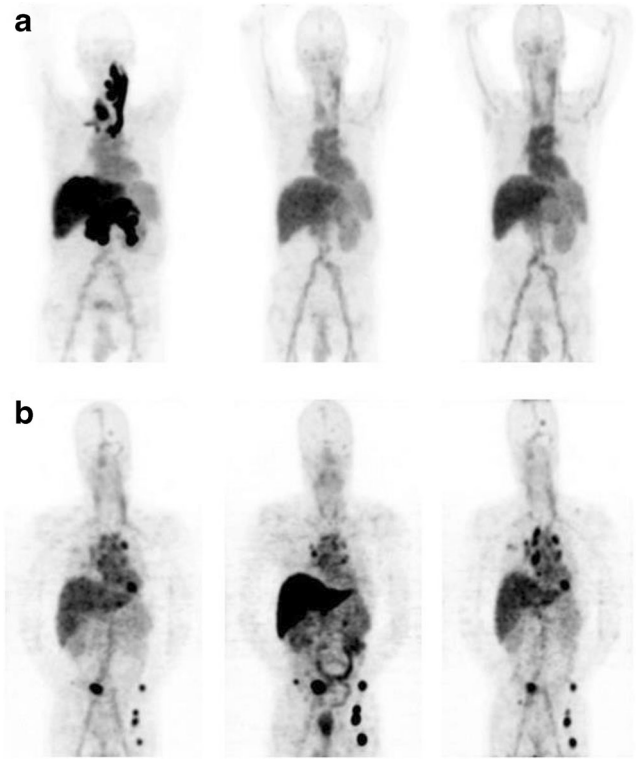

Fig. 9 PET images of heterogeneous ^{89}Zr-bevacizumab accumulation in tumor lesions of metastatic renal cell carcinoma patients. **a** Serial ^{89}Zr-bevacizumab PET scans of patient with RCC metastases in the pancreas, liver, and thyroid, with associated jugular and portal vein thrombosis at baseline (left) and 2 (middle) and 6 weeks (right) after the start of bevacizumab/IFNα. **b** Serial ^{89}Zr-bevacizumab PET scans of patient with RCC metastases in the lungs, mediastinal lymph nodes, bone, and brain at baseline (left) and 2 (middle) and 6 weeks (right) after the start of sunitinib—that is, after 2 sunitinib-free weeks. Reprinted with permission from ref. 54. Copyright 2015 Society of Nuclear Medicine

research using PET, such as ^{68}Ga. In particular, development of new coordinate chemistry for ^{89}Zr labeling has led to wider application of ^{89}Zr in clinical studies. In oncology, ^{89}Zr-immuno-PET techniques have significantly enhanced tumor detection and the efficiency of treatment. Until now, there has been no standard scale for the use of ^{89}Zr. Thus, some image processing steps, including measurements of tumor uptake and data analysis, should be validated and standardized for wider usage. Overall, based on previous studies, it can be expected that ^{89}Zr will be more successfully applied to the diagnosis and treatment of patients via ^{89}Zr-immuno-PET in the future.

Acknowledgements This work was supported by Basic Science Research Program through the National Research Foundation of Korea (NRF) funded by the Ministry of Education (2018R1D1A1B07047572).

Compliance with Ethical Standards

Conflicts of Interest Minh Thanh La, Van Hieu Tran, and Hee-Kwon Kim declare that they have no conflict of interest.

Ethical Approval This article does not contain any studies with animals or human participants performed by any of the authors.

Informed Consent None.

Publisher's Note Springer Nature remains neutral with regard to jurisdictional claims in published maps and institutional affiliations.

References

1. Kasbollah A, Eu P, Cowell S, Deb P. Review on production of ^{89}Zr in a medical cyclotron for PET radiopharmaceuticals. J Nucl Med Technol. 2013;41:35–41.
2. Zweit J, Downey S, Sharma HL. Production of no-carrier-added zirconium-89 for positron emission tomography. Appl Radiat Isot. 1991;42:199–201.
3. Tang Y, Li S, Yang Y, Chen W, Wei H, Wang G, et al. A simple and convenient method for production of ^{89}Zr with high purity. Appl Radiat Isot. 2016;118:326–30.
4. Link JM, Krohn KA, Eary JF, Kishore R, Lewellen TK, Johnson MW, et al. ^{89}Zr for antibody labeling and positron emission tomography. J Labeled Compd Radiopharm. 1986;23:1297–8.
5. Dejesus OT, Nickles RJ. Production and purification of ^{89}Zr, a potential PET antibody label. Int J Rad Appl Instrum A. 1990;41:789–90.
6. Holland JP, Sheh Y, Lewis JS. Standardized methods for the production of high specific-activity zirconium-89. Nucl Med Biol. 2009;36:729–39.
7. Walther M, Gebhardt P, Grosse-Gehling P, Würbach L, Irmler I, Preusche S, et al. Implementation of ^{89}Zr production and in vivo imaging of B-cells in mice with ^{89}Zr-labeled anti-B-cell antibodies by small animal PET/CT. Appl Radiat Isot. 2011;69:852–7.
8. Siikanen J, Tran TA, Olsson TG, Strand SE, Sandell A. A solid target system with remote handling of irradiated targets for PET cyclotrons. Appl Radiat Isot. 2014;94:294–301.
9. Meijs WE, Herscheid JDM, Haisma HJ, Wijbrandts R, van Langevelde F, Van Leuffen PJ, et al. Production of highly pure no-carrier added ^{89}Zr for the labelling of antibodies with a positron emitter. Appl Radiat Isot. 1994;45:1143–7.
10. Queern SL, Aweda TA, Massicano AVF, Clanton NA, El Sayed R, Sader JA, et al. Production of Zr-89 using sputtered yttrium coin targets. Nucl Med Biol. 2017;50:11–6.
11. Pandey MK, Engelbrecht HP, Byrne JF, Packard AB, DeGrado TR. Production of ^{89}Zr via the ^{89}Y(p,n)^{89}Zr reaction in aqueous solution: effect of solution composition on in-target chemistry. Nucl Med Biol. 2014;41:309–16.
12. Uddin MS, Khandaker MU, Kim KS, Lee YS, Lee MW, Kim GN. Excitation functions of the proton induced nuclear reactions on natural zirconium. Nucl Inst Meth Phys Res B. 2008;266:13–20.
13. Kandil SA, Spahn I, Scholten B, Saleh ZA, Saad SMM, Coenen HH, et al. Excitation functions of (α,xn) reactions on ^{nat}Rb and ^{nat}Sr from threshold up to 26MeV: possibility of production of ^{87}Y, ^{88}Y and ^{89}Zr. Appl Radiat Isot. 2007;65:561–8.
14. Lewis VE, Zieba KJ. A transfer standard for d + t neutron fluence and energy. Nucl Inst Meth. 1980;174:141–4.
15. Sadeghi M, Enferadi M, Bakhtiari M. Accelerator production of the positron emitter zirconium-89. Ann Nucl Energy. 2012;41:97–103.
16. Holland JP, Divilov V, Bander NH, Smith-Jones PM, Larson SM, Lewis JS. ^{89}Zr-DFO-J591 for immunoPET of prostate-specific membrane antigen expression in vivo. J Nucl Med. 2010;51:1293–300.

17. Meijs WE, Haisma HJ, Van Der Schors R, Wijbrandts R, Van Den Oever K, Klok RP, et al. A facile method for the labeling of proteins with zirconium isotopes. Nucl Med Biol. 1996;23:439–48.
18. Verel I, Visser GWM, Boellaard R, Stigter-van Walsum M, Snow GB, van Dongen GAMS. ^{89}Zr immuno-PET: comprehensive procedures for the production of ^{89}Zr-labeled monoclonal antibodies. J Nucl Med. 2003;44:1271–81.
19. Lewis MR, Shively JE. Maleimidocysteineamido-DOTA derivatives: new reagents for radiometal chelate conjugation to antibody sulfhydryl groups undergo pH-dependent cleavage reactions. Bioconjug Chem. 1998;9:72–86.
20. Perk LR, Vosjan MJWD, Visser GWM, Budde M, Jurek P, Kiefer GE, et al. *p*-Isothiocyanatobenzyl-desferrioxamine: a new bifunctional chelate for facile radiolabeling of monoclonal antibodies with zirconium-89 for immuno-PET imaging. Eur J Nucl Med Mol Imaging. 2010;37:250–9.
21. Vosjan MJWD, Perk LR, Visser GWM, Budde M, Jurek P, Kiefer GE, et al. Conjugation and radiolabeling of monoclonal antibodies with zirconium-89 for PET imaging using the bifunctional chelate p-isothiocyanatobenzyl-desferrioxamine. Nat Protoc. 2010;5:739.
22. Gao F, Ieritano C, Chen KT, Dias GM, Rousseau J, Bénard F, et al. Two bifunctional desferrioxamine chelators for bioorthogonal labeling of biovectors with zirconium-89. Org Biomol Chem. 2018;16:5102–6.
23. White DL, Durbin PW, Jeung N, Raymond KN. Specific sequestering agents for the actinides. 16. Synthesis and initial biological testing of polydentate oxohydroxypyridinecarboxylate ligands. J Med Chem. 1988;31:11–8.
24. Allott L, Da Pieve C, Meyers J, Spinks T, Ciobota DM, Kramer-Marek G, et al. Evaluation of DFO-HOPO as an octadentate chelator for zirconium-89. Chem Commun. 2017;53:8529–32.
25. Patra M, Bauman A, Mari C, Fischer CA, Blacque O, Häussinger D, et al. An octadentate bifunctional chelating agent for the development of stable zirconium-89 based molecular imaging probes. Chem Commun. 2014;50:11523–5.
26. Vugts DJ, Klaver C, Sewing C, Poot AJ, Adamzek K, Huegli S, et al. Comparison of the octadentate bifunctional chelator DFO*-*p*Phe-NCS and the clinically used hexadentate bifunctional chelator DFO-*p*Phe-NCS for ^{89}Zr-immuno-PET. Eur J Nucl Med Mol Imaging. 2017;44:286–95.
27. Guérard F, Lee Y-S, Tripier R, Szajek LP, Deschamps JR, Brechbiel MW. Investigation of Zr(iv) and ^{89}Zr(iv) complexation with hydroxamates: progress towards designing a better chelator than desferrioxamine B for immuno-PET imaging. Chem Commun. 2013;49:1002–4.
28. Rousseau J, Zhang Z, Wang X, Zhang C, Lau J, Rousseau E, et al. Synthesis and evaluation of bifunctional tetrahydroxamate chelators for labeling antibodies with ^{89}Zr for imaging with positron emission tomography. Bioorganic Med Chem Lett. 2018;28:899–905.
29. Zhai C, Summer D, Rangger C, Franssen GM, Laverman P, Haas H, et al. Novel bifunctional cyclic chelator for ^{89}Zr labeling–radiolabeling and targeting properties of RGD conjugates. Mol Pharm. 2015;12:2142–50.
30. Adams CJ, Wilson JJ, Boros E. Multifunctional desferrichrome analogues as versatile ^{89}Zr(IV) chelators for immunoPET probe development. Mol Pharm. 2017;14:2831–42.
31. Liu S, Edwards DS. Bifunctional chelators for therapeutic lanthanide radiopharmaceuticals. Bioconjug Chem. 2001;12:7–34.
32. Seibold U, Wängler B, Wängler C. Rational design, development, and stability assessment of a macrocyclic four-hydroxamate-bearing bifunctional chelating agent for ^{89}Zr. Chem Med Chem. 2017;12:1555–71.
33. Deri MA, Ponnala S, Zeglis BM, Pohl G, Dannenberg JJ, Lewis JS, et al. Alternative chelator for ^{89}Zr radiopharmaceuticals: radiolabeling and evaluation of 3,4,3-(LI-1,2-HOPO). J Med Chem. 2014;57:4849–60.
34. Bhatt NB, Pandya DN, Xu J, Tatum D, Magda D, Wadas TJ. Evaluation of macrocyclic hydroxyisophthalamide ligands as chelators for zirconium-89. PLoS One. 2017;12:e0178767–e77.
35. Wadas TJ, Wong EH, Weisman GR, Anderson CJ. Coordinating radiometals of copper, gallium, indium, yttrium, and zirconium for PET and SPECT imaging of disease. Chem Rev. 2010;110:2858–902.
36. Pandya DN, Bhatt N, Yuan H, Day CS, Ehrmann BM, Wright M, et al. Zirconium tetraazamacrocycle complexes display extraordinary stability and provide a new strategy for zirconium-89-based radiopharmaceutical development. Chem Sci. 2017;8:2309–14.
37. Börjesson PKE, Jauw YWS, Boellaard R, de Bree R, Comans EFI, Roos JC, et al. Performance of immuno–positron emission tomography with zirconium-89-labeled chimeric monoclonal antibody U36 in the detection of lymph node metastases in head and neck cancer patients. Clin Cancer Res. 2006;12:2133–40.
38. Rizvi SN, Visser OJ, Vosjan MJ, van Lingen A, Hoekstra OS, Zijlstra JM, et al. Biodistribution, radiation dosimetry and scouting of ^{90}Y-ibritumomab tiuxetan therapy in patients with relapsed B-cell non-Hodgkin's lymphoma using ^{89}Zr-ibritumomab tiuxetan and PET. Eur J Nucl Med Mol Imaging. 2012;39:512–20.
39. Gaykema SBM, Brouwers AH, Lub-de Hooge MN, Pleijhuis RG, Timmer-Bosscha H, Pot L, et al. ^{89}Zr-bevacizumab PET imaging in primary breast cancer. J Nucl Med. 2013;54:1014–8.
40. van Asselt SJ, Oosting SF, Brouwers AH, Bongaerts AHH, de Jong JR, Lub-de Hooge MN, et al. Everolimus reduces ^{89}Zr-bevacizumab tumor uptake in patients with neuroendocrine tumors. J Nucl Med. 2014;55:1087–92.
41. den Hollander MW, Bensch F, Glaudemans AW, Oude Munnink TH, Enting RH, den Dunnen WF, et al. TGF-β antibody uptake in recurrent high-grade glioma imaged with ^{89}Zr-fresolimumab PET. J Nucl Med. 2015;56:1310–4.
42. Lamberts LE, Menke-van der Houven van Oordt CW, ter Weele EJ, Bensch F, Smeenk MM, Voortman J, et al. ImmunoPET with anti-mesothelin antibody in patients with pancreatic and ovarian cancer before anti-mesothelin antibody–drug conjugate treatment. Clin Cancer Res. 2016;22:1642–52.
43. van Loon J, Even AJG, Aerts HJWL, Öllers M, Hoebers F, van Elmpt W, et al. PET imaging of zirconium-89 labelled cetuximab: a phase I trial in patients with head and neck and lung cancer. Radiother Oncol. 2017;122:267–73.
44. Jauw YWS, Zijlstra JM, de Jong D, Vugts DJ, Zweegman S, Hoekstra OS, et al. Performance of ^{89}Zr-labeled-rituximab-PET as an imaging biomarker to assess CD20 targeting: a pilot study in patients with relapsed/refractory diffuse large B cell lymphoma. PLoS One. 2017;12:e0169828.
45. Bensch F, Lamberts LE, Smeenk MM, Jorritsma-Smit A, Lub-de Hooge MN, Terwisscha van Scheltinga AGT, et al. ^{89}Zr lumretuzumab PET imaging before and during HER3 antibody lumretuzumab treatment in patients with solid tumors. Clin Cancer Res. 2017;23:6128–37.
46. van Es SC, Brouwers AH, Mahesh SVK, Leliveld-Kors AM, de Jong IJ, Lub-de Hooge MN, et al. ^{89}Zr-bevacizumab PET: potential early read out for efficacy of everolimus in metastatic renal cell carcinoma patients. J Nucl Med. 2017;58:905–10.
47. Bensch F, Brouwers AH, Lub-de Hooge MN, de Jong JR, van der Vegt B, Sleijfer S, et al. ^{89}Zr-trastuzumab PET supports clinical decision making in breast cancer patients, when HER2 status cannot be determined by standard work up. Eur J Nucl Med Mol Imaging. 2018;45:2300–6.
48. Bensch F, van der Veen EL, Lub-de Hooge MN, Jorritsma-Smit A, Boellaard R, Kok IC, et al. ^{89}Zr-atezolizumab imaging as a non-invasive approach to assess clinical response to PD-L1 blockade in cancer. Nat Med. 2018;24:1852–8.

49. Ulaner GA, Hyman DM, Ross DS, Corben A, Chandarlapaty S, Goldfarb S, et al. Detection of HER2-positive metastases in patients with HER2-negative primary breast cancer using ^{89}Zr-trastuzumab PET/CT. J Nucl Med. 2016;57:1523–8.
50. Moja L, Tagliabue L, Balduzzi S, Parmelli E, Pistotti V, Guarneri V, et al. Trastuzumab containing regimens for early breast cancer. Cochrane Database of Syst Rev. 2012.
51. Gong J, Liu T, Fan Q, Bai L, Bi F, Qin S, et al. Optimal regimen of trastuzumab in combination with oxaliplatin/capecitabine in first-line treatment of HER2-positive advanced gastric cancer (CGOG1001): a multicenter, phase II trial. BMC Cancer. 2016;16:68.
52. Gaykema SBM, Schröder CP, Vitfell-Rasmussen J, Chua S, Oude Munnink TH, Brouwers AH, et al. ^{89}Zr-trastuzumab and ^{89}Zr-bevacizumab PET to evaluate the effect of the HSP90 inhibitor NVP-AUY922 in metastatic breast cancer patients. Clin Cancer Res. 2014;20:3945–54.
53. Bahce I, Huisman MC, Verwer EE, Ooijevaar R, Boutkourt F, Vugts DJ, et al. Pilot study of ^{89}Zr-bevacizumab positron emission tomography in patients with advanced non-small cell lung cancer. EJNMMI Res. 2014;4:35.
54. Oosting SF, Brouwers AH, van Es SC, Nagengast WB, Oude Munnink TH, Lub-de Hooge MN, et al. ^{89}Zr-bevacizumab PET visualizes heterogeneous tracer accumulation in tumor lesions of renal cell carcinoma patients and differential effects of antiangiogenic treatment. J Nucl Med. 2015;56:63–9.
55. Oordt CWM-vH, Gootjes EC, Huisman MC, Vugts DJ, Roth C, Luik AM, et al. ^{89}Zr-cetuximab PET imaging in patients with advanced colorectal cancer. Oncotarget. 2015;6:30384–93.
56. Pandit-Taskar N, O'Donoghue JA, Beylergil V, Lyashchenko S, Ruan S, Solomon SB, et al. ^{89}Zr-huJ591 immuno-PET imaging in patients with advanced metastatic prostate cancer. Eur J Nucl Med Mol Imaging. 2014;41:2093–105.
57. ter Weele EJ, Terwisscha van Scheltinga AGT, Kosterink JGW, Pot L, Vedelaar SR, Lamberts LE, et al. Imaging the distribution of an antibody-drug conjugate constituent targeting mesothelin with ^{89}Zr and IRDye 800CW in mice bearing human pancreatic tumor xenografts. Oncotarget. 2015;6:42081–90.